J Mater Sci: Mater Med (2015) 26:74
DOI 10.1007/s10856-015-5411-9

BIOCOMPATIBILITY STUDIES

Porous bioactive scaffolds: characterization and biological performance in a model of tibial bone defect in rats

Hueliton Wilian Kido · Carla Roberta Tim · Paulo Sérgio Bossini · Nivaldo Antônio Parizotto · Cynthia Aparecida de Castro · Murilo Camuri Crovace · Ana Candida Martins Rodrigues · Edgar Dutra Zanotto · Oscar Peitl Filho · Fernanda de Freitas Anibal · Ana Claudia Muniz Rennó

Received: 5 May 2014 / Accepted: 6 November 2014

Abstract The aim of this study was to evaluate the effects of highly porous Biosilicate® scaffolds on bone healing in a tibial bone defect model in rats by means of histological evaluation (histopathological and immunohistochemistry analysis) of the bone callus and the systemic inflammatory response (immunoenzymatic assay). Eighty Wistar rats (12 weeks-old, weighing ±300 g) were randomly divided into 2 groups (n = 10 per experimental group, per time point): control group and Biosilicate® group (BG). Each group was euthanized 3, 7, 14 and 21 days post-surgery. Histological findings revealed a similar inflammatory response in both experimental groups, 3 and 7 days post-surgery. During the experimental periods (3–21 days post-surgery), it was observed that the biomaterial degradation, mainly in the periphery region, provided the development of the newly formed bone into the scaffolds. Immunohistochemistry analysis demonstrated that the Biosilicate® scaffolds stimulated cyclooxygenase-2, vascular endothelial growth factor and runt-related transcription factor 2 expression. Furthermore, in the immunoenzymatic assay, BG presented no difference in the level of tumor necrosis factor alpha in all experimental periods. Still, BG showed a higher level of interleukin 4 after 14 days post-implantation and a lower level of interleukin 10 in 21 days post-surgery. Our results demonstrated that Biosilicate® scaffolds can contribute for bone formation through a suitable architecture and by stimulating the synthesis of markers related to the bone repair.

H. W. Kido · C. R. Tim · N. A. Parizotto
Department of Physiotherapy, Post-Graduate Program of Biotechnology, Federal University of São Carlos (UFSCar), São Carlos, SP, Brazil
e-mail: hueliton_kido@yahoo.com.br

P. S. Bossini · A. C. M. Rennó (✉)
Department of Biosciences, Federal University of São Paulo (UNIFESP), Ana Costa, 95, Santos, SP, Brazil
e-mail: a.renno@unifesp.br

C. A. de Castro
Department of Physiological Sciences, Federal University of São Carlos (UFSCar), São Carlos, SP, Brazil

M. C. Crovace · A. C. M. Rodrigues · E. D. Zanotto · O. P. Filho
Department of Materials Engineering, Vitreous Materials Laboratory (LaMaV), Federal University of São Carlos (UFSCar), São Carlos, SP, Brazil

F. de Freitas Anibal
Department of Morphology and Pathology, Federal University of São Carlos (UFSCar), São Carlos, SP, Brazil

1 Introduction

Although bone tissues have the ability of healing themselves, multiple factors may impair fracture consolidation, including fractures beyond critical size dimension, bone loss caused by diseases, infections or tumor resections, which may lead to the development of pseudoarthosis or even non-union fractures [1]. In this context, several surgical procedures are required to treat such clinical conditions, which are related to considerable morbidity and increased health care needs [2]. Bone grafts to enhance bone repair have been emerging as a promising alternative and include the use of autografts, allografts and synthetic bone substitutes [3–5].

Nevertheless, the limited availability of autogenous bone implants and the possibility of infectious diseases or tissue rejection associated to the use of allogenous implants are pivotal restrictions related to bone healing therapies [6].

Published online: 29 January 2015

As an alternative, synthetic bone substitutes such as calcium phosphate (CaP) ceramics [7], polymer-based materials [8], bioactive glass and glass–ceramics [9] have been developed in order to overcome these limitations [10–12].

Bioactive glasses are a well-known class of materials, with a markedly osteogenic potential, able of stimulating bone metabolism and accelerating bone healing [13–15]. These materials when immersed in body fluids promote release of ions in the medium, leading to the formation of a porous layer which is rich in silica, followed by the formation of hydroxy carbonate-apatite (HCA) layer on the surface of the material [16]. The formation of the HCA layer may contribute to the development of bone tissue, once the HCA is equivalent to inorganic mineral phase of bone [16].

Despite the osteogenic potential of the bioactive glasses, their use has been limited because of their poor mechanical properties and very high crystallization tendency when heated [17]. As an alternative, some glass–ceramics obtained by controlled crystallization of certain glasses based on the quaternary Na_2O–CaO–SiO_2–P_2O_5 system having improved mechanical properties, including Biosilicate®, have been developed [17]. It was demonstrated that Biosilicate® is biocompatible with bone tissues and presents non-cytotoxicity [18]. Furthermore, its osteogenic effects have already been demonstrated by using both in vitro and in vivo studies [19–21]. Granito et al. [21] found that Biosilicate® presented higher bone volume when compared to Bioglass 45S5 in a tibial bone defect model in rats 20 days post-surgery.

The current availability of glass ceramics for the treatment of bone defects, including Biosilicate®, is still mainly in solid pieces or in the form of granules. One of the main disadvantages of those forms is that they may not have the proper porosity to allow tissue ingrowth and may not degrade according to the rate of bone tissue formation [22]. In this context, many efforts have been made to develop improved bone graft substitutes that interact more appropriately with the complex biological environment of bone tissue [23]. Biosilicate® porous scaffolds offer a three-dimensional structure which mimics the structure of the extracellular matrix of natural bone, allowing bone cell attachment, proliferation and differentiation at the region of the defect [24].

An initial in vivo study demonstrated that a porous Biosilicate® scaffold (total porosity of 44 %) was able to support bone ingrowth in the region of the tibial bone defect, thus highlighting the osteogenic potential of the material. However, the amount of newly formed bone was not significantly different from the control group which may be related to its relatively low porosity [25].

In order to obtain more appropriate bone substitutes to be used as grafts, highly porous scaffolds may be an interesting alternative with useful properties for biomedical applications, i.e. biodegradability and more appropriate structure to allow tissue ingrowth [26].

In this context, a new Biosilicate® scaffold, with increased porosity (total porosity of 82 %), was developed [18]. It was hypothesized that this innovative osteogenic scaffold would offer a more suitable template for bone cell attraction and tissue ingrowth. Consequently, the present study aimed to evaluate the in vivo orthotopic response of this new porous bioactive scaffold, during different experimental set points (3, 7, 14 and 21 days after implantation) in a tibial bone defect model in rats. Histology and immunohistochemistry analyses of the factors involved in osteogenesis (COX-2, VEGF, Runx2) were used to evaluate the effects of the porous bioactive scaffold in the bone callus. Furthermore, an immunoenzymatic assay was performed to evaluate the action of the material on the systemic inflammatory response by quantifying the inflammatory cytokines levels (IL-4, IL-10 and TNF-α) in rat serum.

2 Materials and methods

2.1 Fabrication and characterization of the Biosilicate® scaffolds

Biosilicate® was obtained by melting reagent grade raw materials (Na_2CO_3—JT Baker, $CaCO_3$—JT Baker, Na_2HPO_4—JT Baker, and SiO2—Zetasil 2) in a platinum crucible at 1250 °C for 4 h. The glass was poured in a stainless steel mould and heat treated until it reached full crystallization in an electric furnace. More details of the synthesis of Biosilicate® are described in the WO 2004/074199 patent [27]. Glass pieces were crushed in a porcelain mortar and milled in a planetary ball mill at 550 rpm for 240 min. In this study, the Biosilicate® scaffolds were manufactured by a method based in the addition of a porogen agent. This method was described with details in a previous work [18, 28]. This method is therefore only shortly described here: initially, 100 ml of a suspension containing 67 vol% of isopropyl alcohol anhydrous (QHEMIS), 3 vol% of polyvinyl butiral (Butvar B-98), 24 vol% of carbon black (CABOT BP-120), and 6 vol% of Biosilicate® was prepared. Then isopropyl alcohol, PVB, and Biosilicate® were mixed in an agate jar and milled in a planetary ball mill (Pulverisette 6—FRITSCH) at 550 rpm for 1 h. The agate spheres were removed from the suspension and the pre-sieved carbon black (300–600 μm) was added and then mixed for 5 min at 150 rpm. The suspension was poured into a plastic container and dried with a heat gun (DEKEL DK1210). The resulting granulated powder was pressed in two steps, the first unixial

using a cylindrical steel mould and the second isostatical. Finally, the cylindrical samples were heat treated for organics burn-out and to promote Biosilicate® sintering. Scaffolds of approximately 3 mm (diameter) by 2 mm (thickness) were obtained. Sterilization was performed in an electric oven at 130 °C for 14 h.

For microstructural observation, six scaffolds were embedded in epoxy resin (EpoThin®—BUEHLER) under vacuum. The embedded samples were ground in silicon carbide paper until grit size 1200 and polished with cerium oxide. Then, they were coated with a thin layer of gold by sputtering (Quorum Q150R ES) and analyzed in SEM (Philips FEG XL-30). Both transversal and longitudinal sections of the scaffolds were analyzed. The average pore size and total porosity were determined by analysis of SEM images using the software Image-J (version 1.46i).

2.2 Experimental design

This study was conducted according to the Guiding Principles for the Use of Laboratory Animals and it was approved by the Animal Care Committee guidelines at Federal University of São Carlos (protocol 046/2012).

In this investigation, 80 male Wistar rats were used (12 weeks old and weighing 300 g), and were maintained under controlled conditions of temperature (24 ± 2 °C) with light–dark periods of 12 h, with free access to water and commercial diet. The experimental animals were randomly distributed into 2 groups: Control group (CG) and Biosilicate® group (BG). Each group was divided into 4 four subgroups (n = 10 animals) euthanized 3, 7, 14 and 21 days post-surgery.

2.3 Surgical procedures

Before surgery, all the animals were anesthetized by intraperitoneal injection of ketamine (40 mg/kg, Agener®, Brasília, Brazil) and xylazine (20 mg/kg, Syntec®, Cotia, Brazil). After exposing the right proximal tibia of each animal, a standardized 3.0 mm diameter non-critical bone defect was created by using a motorized drill under irrigation with saline solution [21, 25, 29]. The porous bioactive scaffolds were implanted, in the created defects in a randomization scheme. The skin was closed and sutured with 4–0 nylon monofilament (Shalon®, São Luis de Montes Belos, GO, Brazil), and disinfected with povidone iodine. The health status of the animals was monitored on a daily basis.

The animals were housed in pairs and the intake of water and food was monitored in the initial postoperative period. Moreover, the animals were observed for signs of pain, infection and activity. According to each experimental period, animals were euthanized by CO_2 asphyxiation.

The blood and the right tibia of each animal were collected for analysis. The blood samples were used for the quantification of inflammatory factors and the right tibia was taken to histological analyzes.

2.4 Histopathological analysis

The right tibias were fixed in 10 % buffered formalin (Merck, Darmstadt, Germany) for 24 h. Afterwards, the specimens were decalcified in 10 % EDTA solution (ethylenediaminetetraacetic acid, Labsynth®, Diadema, Brazil) for 40 days, dehydrated and embedded in paraffin blocks. Three sections (5 μm) of each specimen were longitudinally sectioned (Microtome Leica Microsystems SP 1600, Nussloch, Germany) and stained with hematoxylin and eosin (H.E. stain, Merck, Darmstadt, Germany). The morphological description of the bone defect was performed with an optical microscopy (Olympus Optical Co., Tokyo, Japan) according to the following parameters: granulation tissue, inflammatory process, area of fibrosis, necrotic tissue, bone formation and biomaterial degradation.

2.5 Immunohistochemistry

Histological sections (5 μm) were deparaffinized using xylene and rehydrated in graded ethanol. After, each specimen was pre-treated in a Steamer with buffer Diva Decloaker (Biocare Medical, CA, USA) for 5 min for antigen retrieval. The material was pre-incubated with 0.3 % hydrogen peroxide (Labsynth®, Diadema, Brazil) in phosphate-buffered saline (PBS) solution for 30 min in order to inactivate endogenous peroxidase and then block with 5 % normal goat serum in PBS solution for 20 min. Three sections of each specimen were incubated for 2 h with polyclonal primary antibody anti-Cyclooxygenase-2, anti-Vascular endothelial growth factor and anti-Runt-related transcription factor 2, all at a concentration of 1:200 (Santa Cruz Biotechnology, Santa Cruz, USA). Afterwards, the sections were incubated with biotin conjugated secondary antibody anti-rabbit IgG (Vector Laboratories, Burlingame, CA, USA) at a concentration of 1:200 in PBS for 30 min, followed by the application of preformed avidin biotin complex conjugated to peroxidase (Vector Laboratories, Burlingame, CA, USA) for 30 min. A solution of 3-3′-diaminobenzidine solution (0.05 %) and Harris hematoxylin were applied.

The expression of cyclooxygenase-2 (COX-2), vascular endothelial growth factor (VEGF) and runt-related transcription factor 2 (Runx2) were assessed qualitatively (presence and location of the immunomarkers) in five predetermined fields using an optical light microscope (Leica Microsystems AG, Wetzlar, Germany). The analysis was performed by 2 observers (CRT and HWK) in a blinded way.

2.6 Immunoenzymatic assay

Quantification of plasma cytokines was performed using the immunoenzymatic assay (ELIZA). In this study, the cytokines interleukin 4 (IL-4), interleukin 10 (IL-10) and tumor necrosis factor alpha (TNF-α) were evaluated by their influences on the inflammatory process [30].

For this purpose, the collected blood from each animal (5 ml) was placed in tubes without anticoagulant for about 2 h until its coagulation. Then, the samples were centrifuged at 1500 rpm for 15 min. The serum that resulted from this centrifugation was aliquoted into microtube and frozen at −80 °C. Cytokines were measured using Duo Set kits (R&D Systems®, Minnesota, USA), following the manufacturer's recommendations. The serum samples were used to measure IL-4, IL-10 and TNF-α. The high affinity microplates were sensitized with monoclonal anti-cytokines and remained "overnight" at room temperature. Afterwards, the plates were blocked (with PBS) and washed. Supernatants and standard curves (made with recombinant cytokines) were added. The plates were maintained at room temperature for 2 h and then another washing was performed. Subsequently, biotinylated anti-cytokine antibodies were added and maintained for 1 h at room temperature. The results were expressed in pg/ml for all cytokines evaluated.

2.7 Statistical analysis

Data were expressed as mean values and standard deviations (SD) for each sample group. The normal distribution of all variables was checked using the Shapiro–Wilk's W test. Two-way ANOVA with Tukey post hoc tests were used to evaluate the variance between groups. All analyses were performed using Excel (2007) and STATISTICA 7.0. For all the tests, the significance level of 5 % ($p < 0.05$) was considered.

3 Results

3.1 Material characterization

The porous bioactive scaffolds which were obtained via addition of carbon black as a porogen agent are highly porous, as can be seen in the images captured via stereomicroscopy (Fig. 1a, b). SEM photomicrographies revealed that the macroporosity was 72 ± 6 %, with an average pore size of 275 μm (Fig. 1c, d). The mechanical strength of the material was sufficient for handling and placing it inside the surgical site.

3.2 General findings

In this study, no animal of CG died and all tibia samples were used for analysis. Only two animals of BG were lost due to a respiratory depression induced by the anesthesia. The other animals rapidly returned to their normal diet and no post-operative complications were observed during the experimental period. At the end of the experiment, 38 tibial implants were retrieved, of which 35 were used for analysis (3 porous bioative scaffolds were lost due to implant fracturing during the histological processing). An overview of the number of implants placed, retrieved and used for analysis is presented in Table 1.

3.3 Histopathological analysis

Representative histological sections of all experimental groups are depicted in Figs. 2 and 3.

3.3.1 3 days

Three days after surgery, histological evaluation of CG revealed that the bone defect area was mostly filled with inflammatory cells and granulation tissue (Fig. 2b). In BG, the integrity of the implant was affected, with material degradation, especially in the borders. The presence of inflammatory cells around the material particles was observed, with ingrowth of granulation tissue (Fig. 2d).

3.3.2 7 days

Seven days after implantation, bone defect area of control animals was filled mostly by granulation tissue, accompanied by some inflammatory cells (Fig. 2f). Furthermore, immature newly formed bone was observed in the periphery of the defect (Fig. 2f). For BG, the degradation of the material continued, leaving lower amounts of material compared to the previous experimental set point (Fig. 2h). Furthermore, in the spaces previously occupied by the material, a discrete inflammatory process and granulation tissue was noticed (Fig. 2h). Newly formed bone was noticed in the contact area between the edges of the bone defect and the remained implant (Fig. 2h).

3.3.3 14 days

For CG, the amount of granulation tissue increased in the bone defect area and some inflammatory cells still could be observed in some specimens (Fig. 3b). In addition, newly formed bone was observed into the area of the defect, mainly at the periphery (Fig. 3b). The degradation of the scaffold had continued, allowing the ingrowth of granulation tissue and newly formed bone (Fig. 3d).

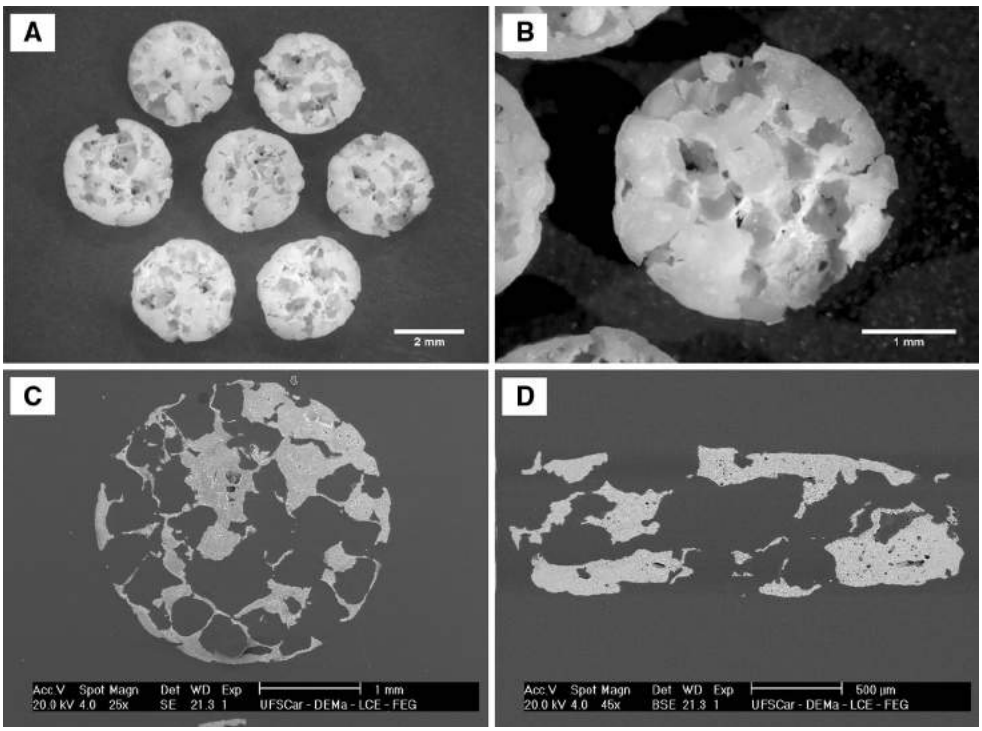

Fig. 1 Images of the Biosilicate® scaffolds obtained with the stereomicroscope Leica MZ75 (**a**, **b**) and SEM images of two scaffolds embedded in epoxy resin under vacuum: longitudinal section (**c**) and transversal section (**d**)

Table 1 Number of implants placed, retrieved and used for histological analyses for the tibial defect implants

	Implants placed				Implants retrieved				Implants used for analysis			
	Day 3	Day 7	Day 14	Day 21	Day 3	Day 7	Day 14	Day 21	Day 3	Day 7	Day 14	Day 21
Tibial implants												
Biosilicate® scaffolds	10	10	10	10	9[a]	9[a]	10	10	8[b]	8[b]	9[b]	10

[a] Deviation from number of implants placed due to animal dead

[b] Deviation from number of implants retrieved due to fracturing of implants during to the histological processing

3.3.4 21 days

After 21 days of implantation, for both experimental groups, bone defect was mostly filled with newly formed bone in both experimental groups (Fig. 3f, h). Some particles of the material could still be noticed the bone defect, mainly in the center of the defect (Fig. 3h).

3.4 Immunohistochemistry

3.4.1 COX-2

COX-2 immunoexpression was observed mainly in the granulation tissue for both experimental groups, 3 and 7 days post-surgery (Fig. 4a, b, c, d). Fourteen days after surgery, for CG and BG, COX-2 expression was observed in the granulation tissue and in the osteoblast cells (Fig. 4e, f). At day 21 after surgery, CG showed COX-2 immunoexpression mainly in the osteoblasts (Fig. 4g). For BG, COX-2 immunoreactivity was detected in the granulation tissue and in the osteocytes (Fig. 4h).

3.4.2 VEGF

Three days after surgery, VEGF immunoreactivity was observed in the granulation tissue in CG and BG (Fig. 5a, b). In this period, for BG, VEGF expression was more evident in the granulation tissue located around the material (Fig. 5b). In the other experimental periods (7, 14 and 21 days), VEGF expression was predominantly detected in the cells involving capillary walls for both groups CG and BG (Fig. 5c, d, e, f, g, h).

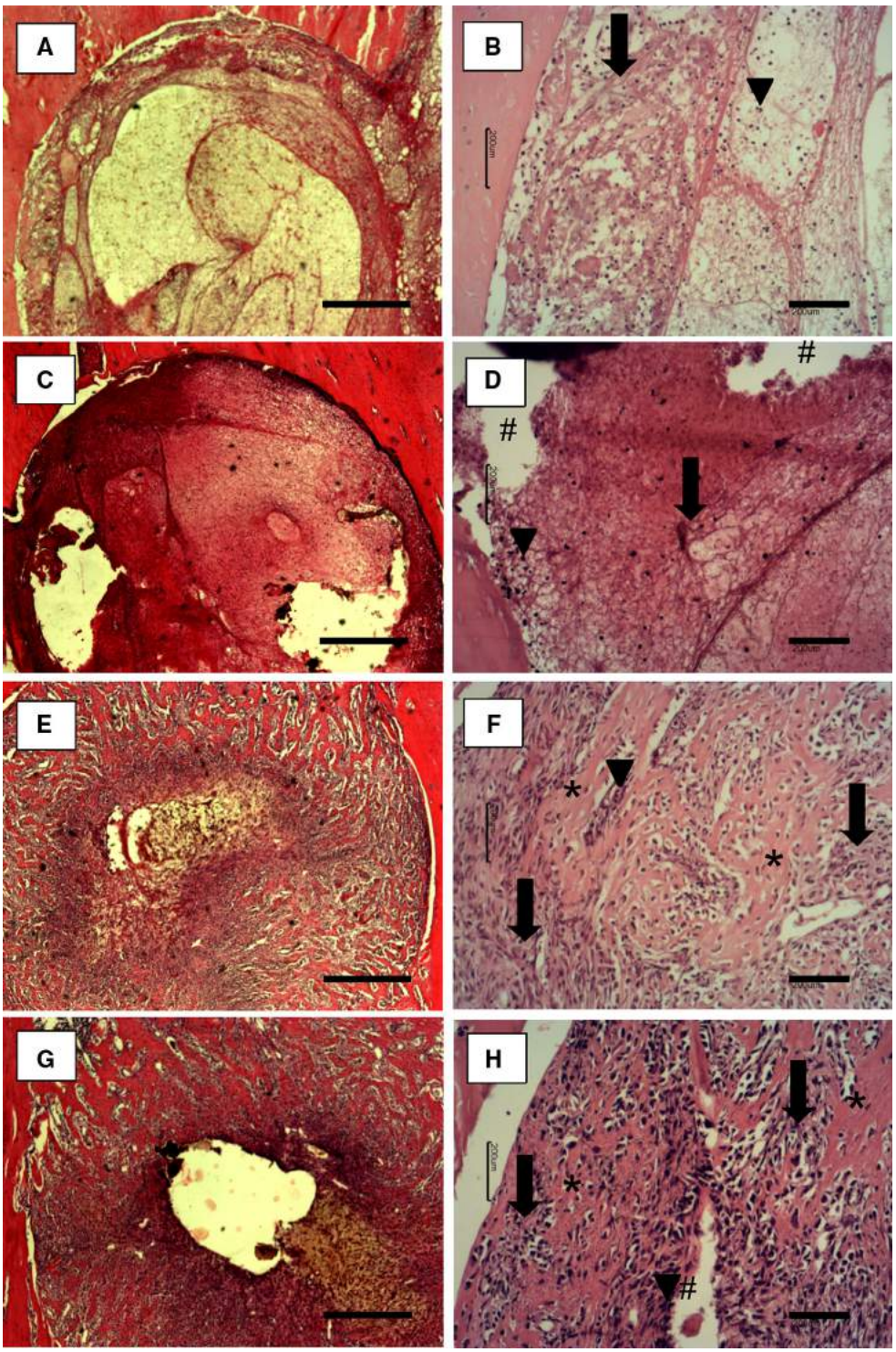

Fig. 2 Representative histological sections of tibial bone defects of the control (CG) and Biosilicate® Group (BG) 3–7 days after surgery: CG 3 days (**a**, **b**), BG 3 days (**c**, **d**), CG 7 days (**e**, **f**), BG 7 days (**g**, **h**). Newly formed bone (*asterisk*), granulation tissue (*black arrow*), infiltrate of inflammatory cells (*filled inverse triangle*) and biomaterial (#). *Bar* represents 500 μm (**a**, **c**, **e**, **g**) and 200 μm (**b**, **d**, **f**, **h**). Hematoxylin and eosin staining

3.4.3 Runx2

Similar to COX-2 and VEGF expression, Runx2 was predominantly detected in the granulation tissue for both CG and BG on day 3 after the surgery (Fig. 6a, b). In the same period, for BG, Runx2 immunoreactivity was mainly observed in the granulation tissue around the material (Fig. 6b). At day 7 after surgery,

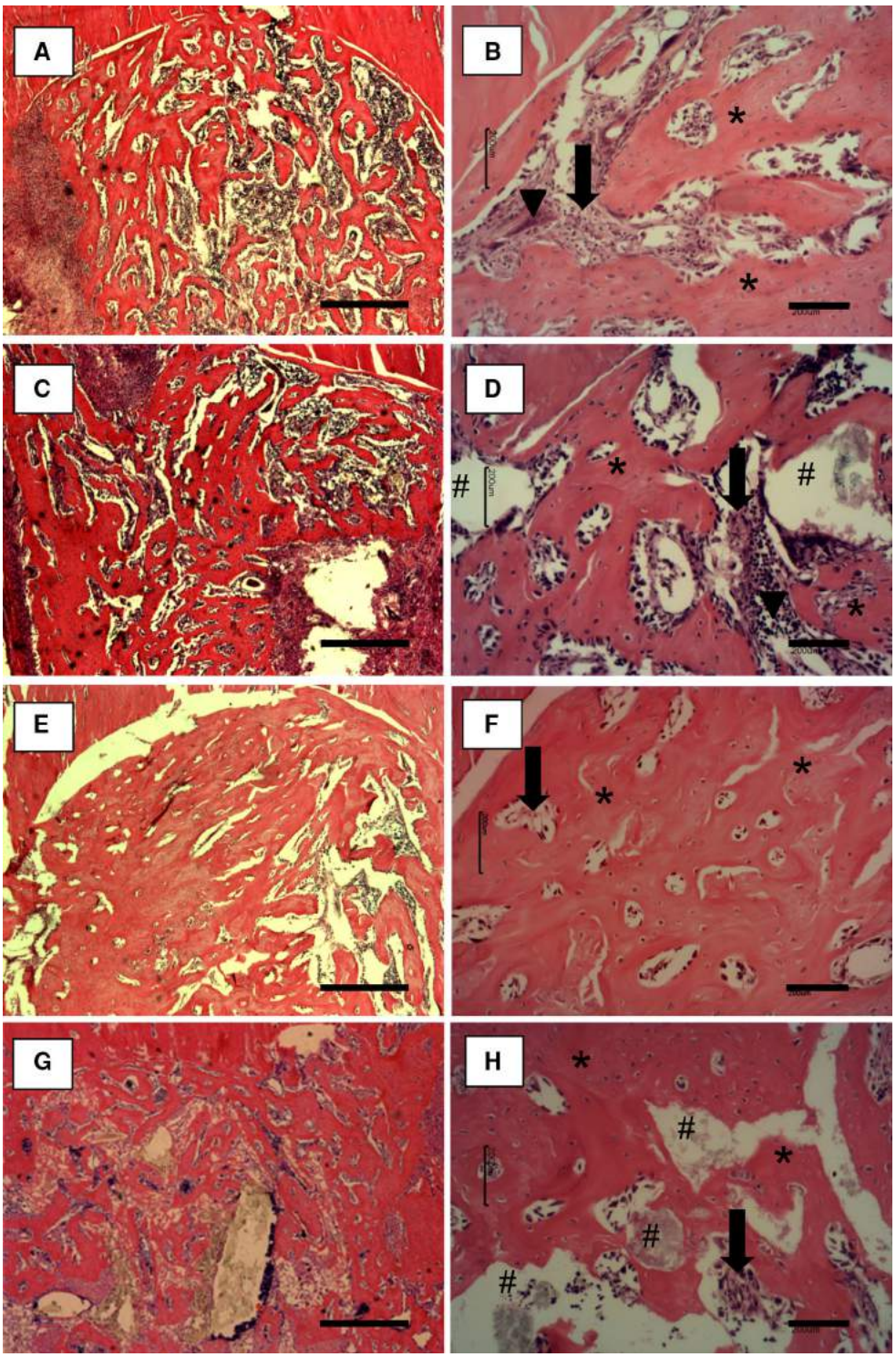

Fig. 3 Representative histological sections of tibial bone defects of the control (CG) and Biosilicate® Group (BG) 14–21 days after surgery: CG 14 days (**a**, **b**), BG 14 days (**c**, **d**), CG 21 days (**e**, **f**), BG 21 days (*g*, *h*). Newly formed bone (*asterisk*), granulation tissue (*black arrow*), infiltrate of inflammatory cells (*filled inverse triangle*) and biomaterial (#). *Bar* represents 500 μm (**a**, **c**, **e**, **g**) and 200 μm (**b**, **d**, **f**, **h**). Hematoxylin and eosin staining

Runx2 immunoexpression was mainly detected in osteoblasts for CG (Fig. 6c) and in the granulation tissue for BG (Fig. 6d). Fourteen and 21 days after surgery, Runx2 expression was detected in osteocytes and osteoblasts for both CG (Fig. 6e, g) and BG (Fig. 6f, h).

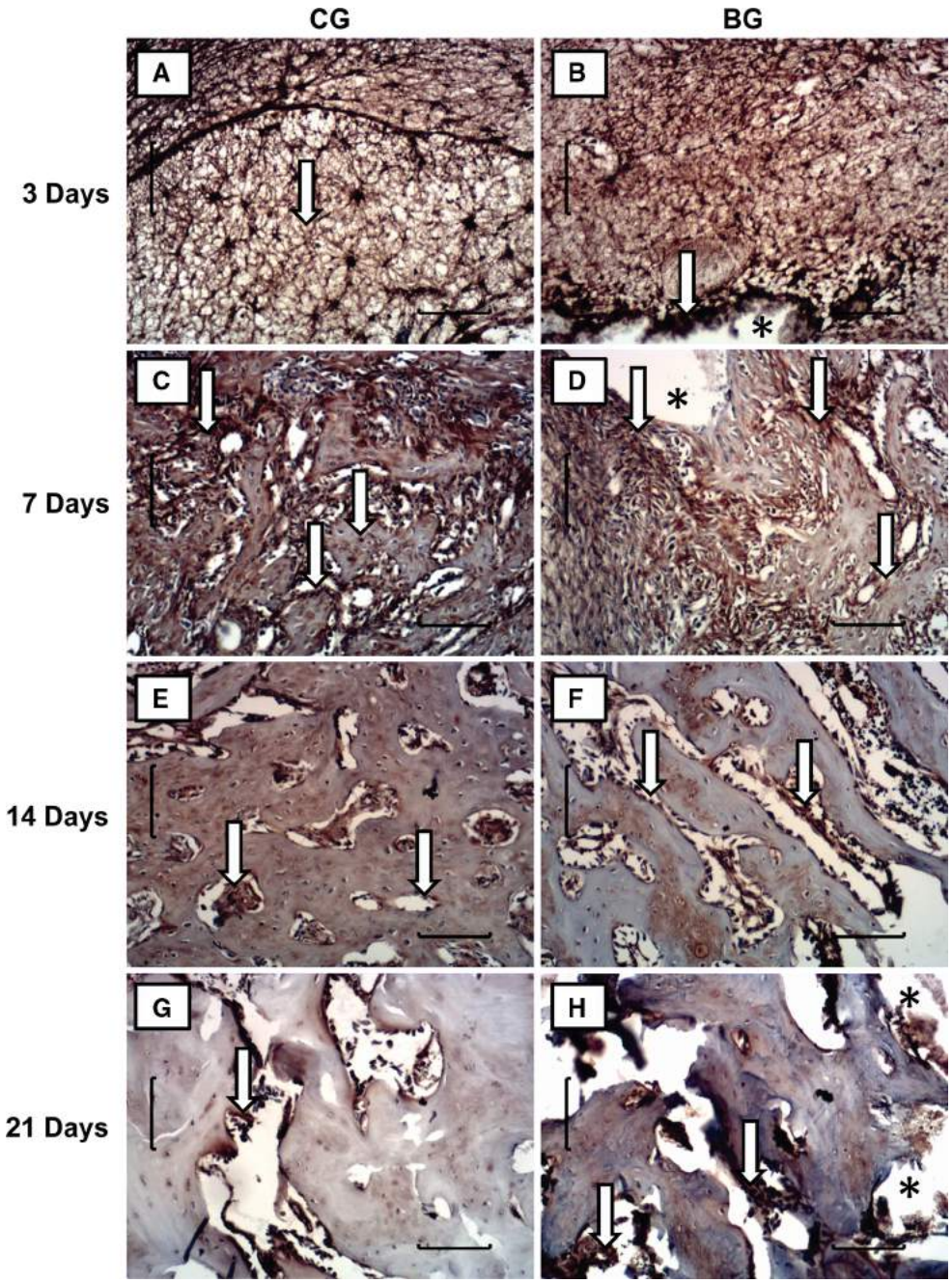

Fig. 4 Representative histological sections of cyclooxygenase-2 (COX-2) immunohistochemistry of the experimental groups (CG and BG) after 3, 7, 14 and 21 days post-surgery: CG 3 days (**a**), BG 3 days (**b**), CG 7 days (**c**), BG 7 days (**d**), CG 14 days (**e**), BG 14 days (**f**), CG 21 days (**g**), BG 21 days (**h**). COX-2 immunoexpression (*arrow*) and biomaterial (#). *Bar* represents 200 μm

3.5 Immunoenzymatic assessment

The immunoenzymatic assessment showed no statistic difference in the levels of TNF-α comparing CG and BG in the experimental periods (Fig. 7). For IL-4, a significantly higher level of this cytokine was observed in BG when compared to CG, 14 days after implantation (Fig. 8). Moreover, the immunoenzymatic evaluation indicated a lower level of IL-10 (Fig. 9) in BG compared to CG, 21 days after the surgery.

4 Discussion

This study aimed to evaluate the biological in vivo response after the implantation of porous bioactive scaffolds in tibial

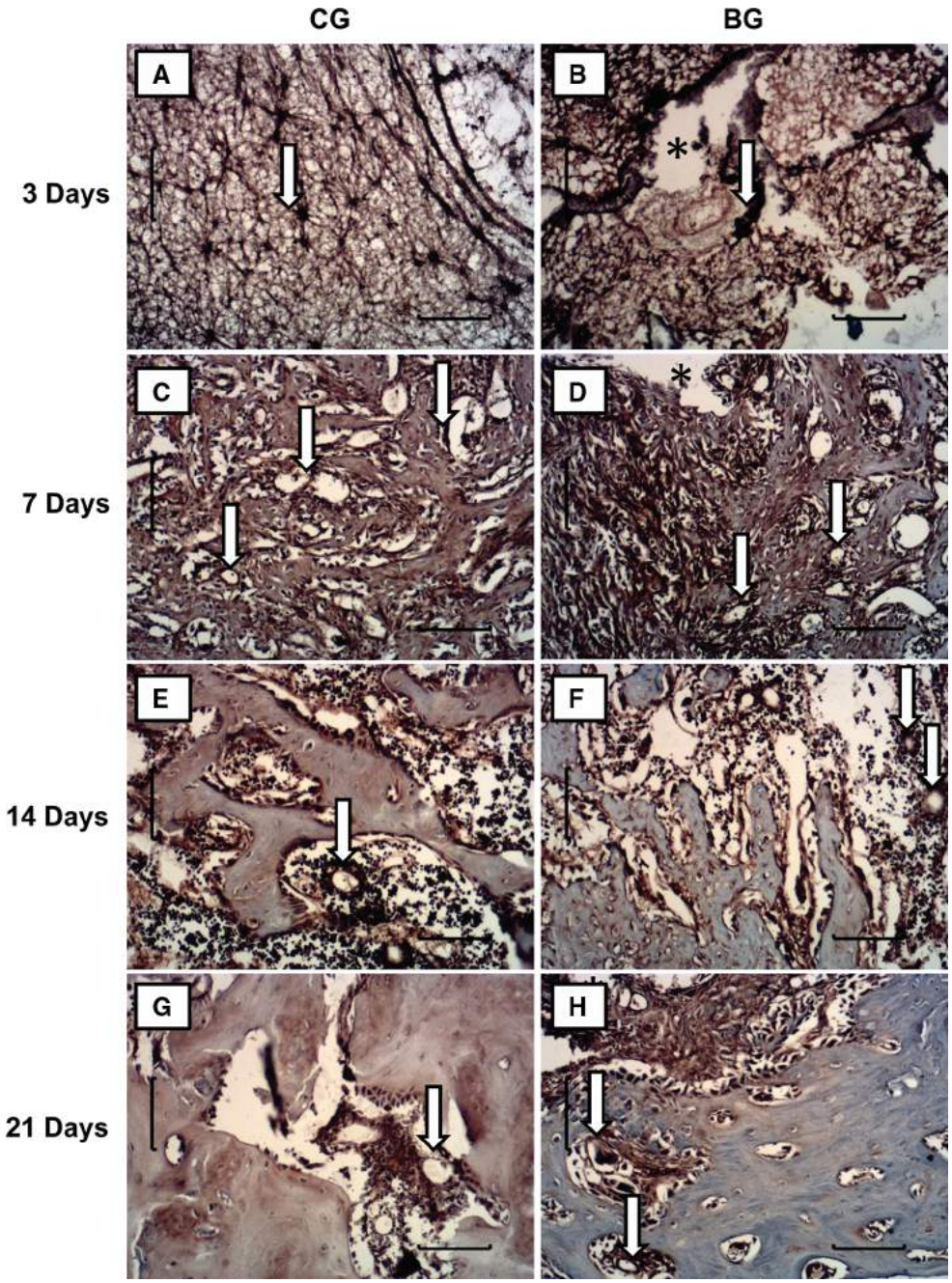

Fig. 5 Representative histological sections of vascular endothelial growth factor (VEGF) immunohistochemistry of the experimental groups (CG and BG) after 3, 7, 14 and 21 days post-surgery: CG 3 days (*a*), BG 3 days (*b*), CG 7 days (*c*), BG 7 days (*d*), CG 14 days (*e*), BG 14 days (*f*), CG 21 days (*g*), BG 21 days (*h*). VEGF immunoexpression (*arrow*) and biomaterial (#). *Bar* represents 200 μm

bone defects in rats after 3, 7, 14 and 21 days. It was hypothesized that increasing the porosity in the bioactive scaffold would have more positive effects on bone tissue formation. The main findings showed that the porous bioactive scaffold degraded over the experimental set points and allowed formation of new bone tissues. In addition, the porous bioactive scaffold induced the immunoexpression of COX-2, VEGF and Runx2 and modulated the synthesis of systemic inflammatory cytokines, with an upregulation of anti-inflammatory cytokines IL-4 and downregulation of the anti-inflammatory cytokine IL-10.

Porous bioactive scaffolds have been of great interest in the bone tissue engineering field to be used as bone substitutes [16, 31, 32]. High bioactivity and adequate scaffold

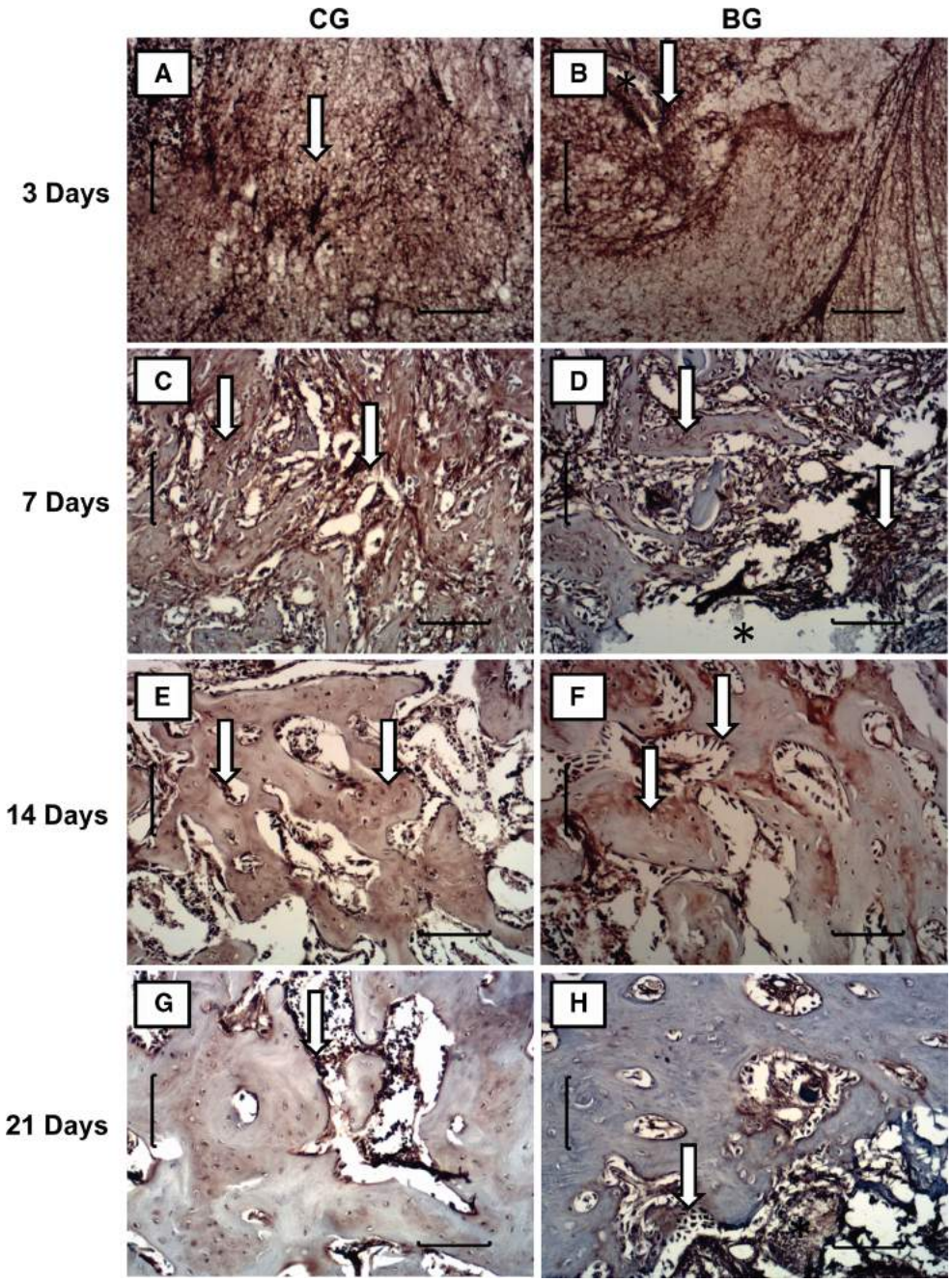

Fig. 6 Representative histological sections of runt-related transcription factor-2 (Runx2) immunohistochemistry of the experimental groups (CG and BG) after 3, 7, 14 and 21 days post-surgery: CG 3 days (**a**), BG 3 days (**b**), CG 7 days (**c**), BG 7 days (**d**), CG 14 days (**e**), BG 14 days (**f**), CG 21 days (**g**), BG 21 days (**h**). Runx2 immunoexpression (*arrow*) and biomaterial (#). *Bar* represents 200 μm

porosity are essential characteristics to stimulate osteoprogenitor cells and to support bone ingrowth [3, 16, 33]. Furthermore, resorption of the material with the same rate of the bone formation is required [34]. Several in vivo studies demonstrated that Biosilicate®, used in powder or scaffolds, was able to stimulate bone metabolism and accelerate the process of bone healing in different animal models, thus highlighting the osteogenic potential of the glass ceramic [25, 35, 36]. These findings are in line with the results of the current study which revealed a continuous newly bone tissue ingrowth at the defect area and in the spaces left by the degraded material. Many studies demonstrated that Biosilicate® scaffolds have bioactive properties [19–21]. Immediately upon the implantation, ions

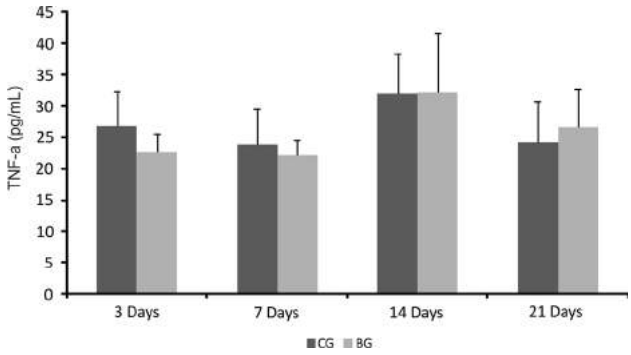

Fig. 7 Levels of TNF-α cytokines evaluated in the serum of rats undergoing implantation of the Biosilicate® scaffolds in different experimental periods

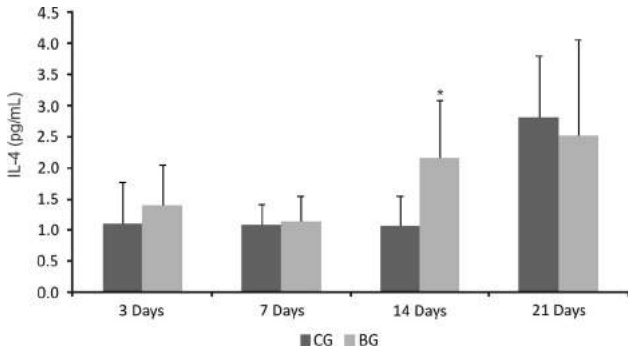

Fig. 8 Levels of IL-4 cytokines evaluated in the serum of rats undergoing implantation of the Biosilicate® scaffolds in different experimental periods. Significant differences of $p < 0.05$ are represented by an *asterisk*

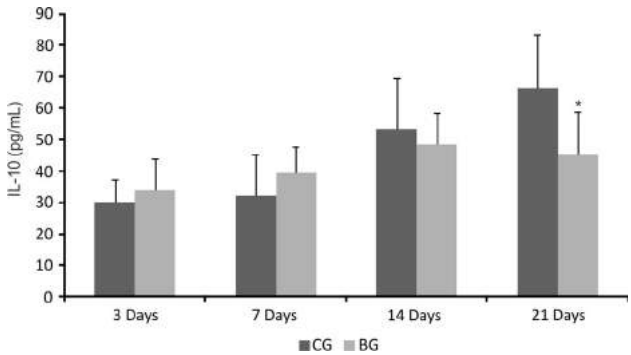

Fig. 9 Levels of IL-10 cytokines evaluated in the serum of rats undergoing implantation of the Biosilicate® scaffolds in different experimental periods. Significant differences of $p < 0.05$ are represented by an *asterisk*

dissolution from the scaffold to bone tissue stimulates the formation of a hydroxyapatite layer, which acts as a template for osteoblast growth, which can affect osteogenesis [16]. Furthermore, high porosity and adequate pore sizes are essential factors for an effective bone substitute material [26]. Scaffolds with pores between of 100–400 μm are of optimal size to allow bone ingrowth and to support neovascularization [37]. The pore size and porosity of the bioactive scaffold used in the present study indicate that it has morphological characteristics which make them suitable to be used as a bone graft.

Moreover, the histological findings demonstrated that the scaffold degraded over time and the degradation happened according to the rate of tissue ingrowth. Besides adequate porosity, proper scaffold degradation is also essential for the process to happen, since formation of new bone tissue needs space to grow in [38].

COX-2, VEGF and Runx2 immunoexpressions were increased in the porous bioactive scaffolds implanted animals. COX-2 and Runx2 have regulatory effects on the proliferation and differentiation of osteoblasts [39, 40], while the VEGF is the most important signal protein produced by cells that stimulates vasculogenesis and angiogenesis [41]. In the current study, the ions released from the scaffolds, such as silicon (Si) and calcium (Ca) may have provided the necessary stimuli to increase the expression of COX-2 and Runx2, and consequently lead to the proliferation of osteoblastic cells. Xynos et al. [33] observed that inorganic particles of Bioglass 45S5®, mainly Si and Ca, may carry specific morphogenic clues that stimulate the proliferation of osteoblastic cells. Furthermore, the increased VEGF expression may be also related to the ions dissolution of the porous bioactive scaffolds. These findings corroborate those of Matsumoto et al. [36] who demonstrated an increased VEGF immunoexpression in the calvaria defects in rabbits after Biosilicate® implantation.

Additionally, severe local and systemic inflammatory responses caused by the implantation of biomaterials may result in delay of the bone healing [34]. The organic response is mainly related to the composition of the material, which may stimulate the expression of inflammatory factors such as interleukins and TNF-α. In the present study, the ELISA assay was used to measure the systemic reaction caused by the porous bioactive scaffold tibial implantation and demonstrated that no significant increase in TNF-α was observed in any experimental group. TNF-α is a factor which is involved in systemic inflammation and is mainly produced by activated macrophages [42]. The fact that the expression of this cytokine did not increase is an indicative that the porous bioactive scaffolds implantation did not induce any systemic inflammatory process.

In addition, porous bioactive scaffolds induced a higher expression of IL-4 on day 14 after implantation and a lower expression of IL-10 on day 21 after surgery. IL-4 and IL-10 are anti-inflammatory cytokines that can regulate the effects of the TNF-α [29]. Cytokines such as IL-4, indirectly promote the bone formation by increasing the

expression of osteoprotegerin (OPG), inhibiting osteoclastogenesis [43]. In this context, the increase of the synthesis of IL-4 cytokines in the scaffold treated animals may have contributed to bone formation.

The results of this initial investigation confirmed our hypothesis that the high porous bioactive scaffold has an adequate porosity structure and is able to support bone tissue ingrowth, thus constituting a promising alternative to be used as bone grafts for tissue engineering. However, in the present study the comparison of the performance of the material was made using an empty control defect model. Future investigations should be performed using standard materials such as calcium phosphate or 45S5 Bioglass. Additionally, the biological performance of the scaffold should be investigated in different bone defect models such as those of critical-size or compromised situations (e.g. osteoporosis).

5 Conclusions

In summary, the results indicated that the porous bioactive scaffold has good adequate porosity and proper degradability and bone-forming properties. The innovative scaffold enhanced the expression of vascular and osteogenic factors and did not induce any systemic inflammatory response. Further long-term studies should be carried out to provide additional information concerning the late stages of material degradation and the bone regeneration induced by the porous scaffold. Moreover, further researches are required to evaluate the biological performance of this new biomaterial in compromised situations to support the use of this promising scaffold for bone engineering applications.

Acknowledgments The authors thank FAPESP (Fundação de Amparo à Pesquisa do Estado de São Paulo) for their financial support.

References

1. Phieffer LS, Goulet JA. Delayed unions of the Tibia. J Bone Joint Surg Am. 2006;88:205–16.
2. Axelrad TW, Kakar S, Einhorn TA. New technologies for the enhancement of skeletal repair. Injury. 2007;38:S49–62.
3. Välimäki V, Yrjans JJ, Vuorio E, Aro HT. Combined effect of bone morphogenetic protein-2 gene therapy and bioactive glass microspheres in enhancement of new bone formation. J Biomed Mater Res. 2005;75:501–9.
4. Drosse I, Volkmer E, Seitz S, Seitz H, Penzkofer R, Zahn K, Matis U, Mutschler W, Augat P, Schieker M. Validation of a femoral critical size defect model for orthotopic evaluation of bone healing: a biomechanical, veterinary and trauma surgical perspective. Tissue Eng Part C Methods. 2008;14:79–88.
5. Bhatt RA, Rozental TD. Bone graft substitutes. Hand Clin. 2012;28:457–68.
6. Nandi SK, Roy S, Mukherjee P, Kundu B, De DK, Basu D. Orthopaedic applications of bone graft and graft substitutes: a review. Indian J Med Res. 2010;132:15–30.
7. Dorozhkin S. Calcium orthophosphate-based biocomposites and hybrid biomaterials. J Mater Sci. 2009;44:2343–87.
8. Hutmacher DW, Schantz JT, Lam CX, Tan KC, Lim TC. State of the art and future directions of scaffold-based bone engineering from a biomaterials perspective. J Tissue Eng Regen Med. 2007;1:245–60.
9. Renno AC, Bossini PS, Crovace MC, Rodrigues AC, Zanotto ED, Parizotto NA. Characterization and in vivo biological performance of biosilicate. Biomed Res Int. 2013;. doi:10.1155/2013/141427.
10. De Long WG Jr, Einhorn TA, Koval K, McKee M, Smith W, Sanders R, Watson T. Bone grafts and bone graft substitutes in orthopaedic trauma surgery. A critical analysis. J Bone Joint Surg Am. 2007;89:649–58.
11. Hak DJ. The use of osteoconductive bone graft substitutes in orthopaedic trauma. J Am Acad Ortho Surg. 2007;15:525–36.
12. Ohtsuki C, Kamitakahara M, Miyazaki T. Bioactive ceramic-based materials with designed reactivity for bone tissue regeneration. J R Soc Interface. 2009;6:S349–60.
13. Hench LL, Xynos ID, Polak JM. Bioactive glasses for in situ tissue regeneration. J Biomater Sci Polym Ed. 2004;15:543–62.
14. Hu YC, Zhong JP. Osteostimulation of bioglass. Chin Med J. 2009;122:2386–9.
15. Xin R, Zhang Q, Gao J. Identification of the wollastonite phase in sintered 45S5 bioglass and its effect on in vitro bioactivity. J Non Cryst Solids. 2010;356:1180–4.
16. Hench LL, Polak JM. Third-generation biomedical materials. Science. 2002;295:1014–7.
17. Peitl Filho O, LaTorre GP, Hench LL. Effect of crystallization on apatite-layer formation of bioactive glass 45S5. J Biomed Mater Res. 1996;30:509–14.
18. Kido HW, Oliveira P, Parizotto NA, Crovace MC, Zanotto ED, Peitl-Filho O, Fernandes KP, Mesquita-Ferrari RA, Ribeiro DA, Renno AC. Histopathological, cytotoxicity and genotoxicity evaluation of Biosilicate® glass-ceramic scaffolds. J Biomed Mater Res A. 2013;101:667–73.
19. Moura J, Teixeira LN, Ravagnani C, Peitl O, Zanotto ED, Beloti MM, Panzeri H, Rosa AL, De Oliveira PT. *In vitro* osteogenesis on a highly bioactive glass–ceramic (Biosilicate®). J Biomed Mater Res A. 2007;82:545–57.
20. Bossini PS, Rennó AC, Ribeiro DA, Fangel R, Peitl O, Zanotto ED, Parizotto NA. Biosilicate® and low-level laser therapy improve bone repair in osteoporotic rats. J Tissue Eng Regen Med. 2011;5:229–37.
21. Granito RN, Renno AC, Ravagnani C, Bossini PS, Mochiuti D, Jorgetti V, Driusso P, Peitl O, Zanotto ED, Parizotto NA, Oishi J. *In vivo* biological performance of a novel highly bioactive glass-ceramic (Biosilicate®): a biomechanical and histomorphometric study in rat tibial defects. J Biomed Mater Res B Appl Biomater. 2011;97:139–47.
22. Wu C, Zhu Y, Chang J, Zhang Y, Xiao Y. Bioactive inorganic-materials/alginate composite microspheres with controllable drug-delivery ability. J Biomed Mater Res B Appl Biomater. 2010;94:32–43.
23. Sachot N, Castaño O, Mateos-Timoneda MA, Engel E, Planell JA. Hierarchically engineered fibrous scaffolds for bone regeneration. J R Soc Interface. 2013;10:20130684.
24. Paşcu EI, Stokes J, McGuinness GB. Electrospun composites of PHBV, silk fibroin and nano-hydroxyapatite for bone tissue engineering. Mater Sci Eng C Mater Biol Appl. 2013;33:4905–16.

25. Pinto KN, Tim CR, Crovace MC, Matsumoto MA, Parizotto NA, Zanotto ED, Peitl O, Renno AC. Effects of Biosilicate® scaffolds and low-level laser therapy on the process of bone healing. Photomed Laser Surg. 2013;31:252–60.
26. Schieker M, Seitz H, Drosse I, Seitz S, Mutschler W. Biomaterials as scaffold for bone tissue engineering. Eur J Trau ma. 2006;32:114–24.
27. Zanotto ED, Ravagnani C, Peitl O, Panzeri H, Lara EH. Process and compositions for preparing particulate, bioactive or resorbable biosilicates for use in the treatment of oral ailments. Sao Carlos: Universidade Federal de Sao Carlos, Universidade de Sao Paulo; 2004. International Classification C03C10/00, WO 2004/074199 (INPI 03006441).
28. Crovace MC. Obtencão de estruturas porosas altamente bioativas via sinterização do Biosilicate®. Dissertation (MSc in Materials Engineering), Post-Graduate Program in Science and Materials Engineering, Federal University of Sao Carlos, Sao Carlos; 2009.
29. Oliveira P, Ribeiro DA, Pipi EF, Driusso P, Parizotto NA, Renno AC. Low-level laser therapy does not modulate the outcomes of a highly bioactive glassceramic (Biosilicate®) on bone consolidation in rats. J Mater Sci Mater Med. 2010;21:1379–84.
30. Pape HC, Marcucio R, Humphrey C, Colnot C, Knobe M, Harvey EJ. Trauma-induced inflammation and fracture healing. J Orthop Trauma. 2010;24:522–5.
31. Gauthier O, Müller R, von Stechow D, Lamy B, Weiss P, Bouler JM, Aguado E, Daculsi G. *In vivo* bone regeneration with injectable calcium phosphate biomaterial: a three-dimensional microcomputed tomographic, biomechanical and SEM study. Biomaterials. 2005;26:5444–53.
32. Link DP, Van den dolder J, Van den Beucken JJJP, Cuijpers VM, Wolke JGC, Mikos AG, Jansen JA. Evaluation of the biocompatibility of calcium phosphate cement/PLGA microparticle composites. J Biomed Mater Res A. 2008;87:760–9.
33. Xynos ID, Edgar AJ, Buttery LDK, Hench LL, Polak JM. Ionic products of bioactive glass dissolution increase proliferation of human osteoblasts and induce insulin-like growth factor II mRNA expression and protein synthesis. Biochem Biophys Res Commun. 2000;276:461–5.
34. Anderson JM, Mcnally AK. Biocompatibility of implants: lymphocyte/macrophage interactions. Semin Immunopathol. 2011; 33:221–33.
35. Granito RN, Ribeiro DA, Rennó AC, Ravagnani C, Bossini PS, Peitl-Filho O, Zanotto ED, Parizotto NA, Oishi J. Effects of biosilicate and bioglass 45S5 on tibial bone consolidation on rats: a biomechanical and a histological study. J Mater Sci Mater Med. 2009;20:2521–6.
36. Matsumoto MA, Holgado LA, Renno ACM, Caviquioli G, Biguetti CC, Saraiva PP, Kawakami RY. A novel bioactive vitroceramic presents similar biological responses as autogenous bone grafts. J Mater Sci Mater Med. 2012;23:1447–56.
37. Karageorgiou V, Kaplan D. Porosity of 3D biomaterial scaffolds and osteogenesis. Biomaterials. 2005;26:5474–91.
38. Salgado AJ, Coutinho OP, Reis RL. Bone tissue engineering: state of the art and future trends. Macromol Biosci. 2004;4: 743–65.
39. Zhang X, Schwarz EM, Young DA, Puzas E, Rosier RN, O'keefe RJ. Cyclo-oxygenase-2 regulates mesenchymal cell differentiation into the osteoblast lineage and is critically involved in bone repair. J. Clin. Invest. 2002;109:1405–15.
40. Komori T. Regulation of skeletal development by the Runx family of transcription factors. J Cell Biochem. 2005;95:445–53.
41. Keramarisa NC, Calorib GM, Nikolaoua VS, Schemitschc EH, Giannoudisa PV. Fracture vascularity and bone healing: a systematic review of the role of VEGF. Injury. 2008;39:S45–57.
42. Hallab NJ, Jacobs JJ. Biologic Effects of Implant Debris. Bull NYU Joint Dis. 2009;67:182–8.
43. Shioi A, Teitelbaum SL, Ross FP, Welgus HG, Suzuki H, Ohara J, Lacey DL. Interleukin 4 inhibits murine osteoclast formation *in vitro*. J Cell Biochem. 1991;47:272–7.